

Properties of Median-Dual Regions on Triangulations in \mathbb{R}^4 with Extensions to Higher Dimensions

David M. Williams¹ ✉ 

Department of Mechanical Engineering, Pennsylvania State University, University Park, Pennsylvania, 16801, United States of America

Hiroaki Nishikawa ✉

National Institute of Aerospace, Hampton, Virginia 23666, United States

Abstract

Many time-dependent problems in the field of computational fluid dynamics can be solved in a four-dimensional space-time setting. However, such problems are computationally expensive to solve using modern high-order numerical methods. In order to address this issue, efficient, node-centered edge-based schemes are currently being developed. In these schemes, a median-dual tessellation of the space-time domain is constructed based on an initial triangulation. Unfortunately, it is not straightforward to construct median-dual regions or deduce their properties on triangulations for $d \geq 4$. In this work, we provide the first rigorous definition of median-dual regions on triangulations in any number of dimensions. In addition, we present the first methods for calculating the geometric properties of these dual regions. We introduce a new method for computing the hypervolume of a median-dual region in \mathbb{R}^d . Furthermore, we provide a new approach for computing the directed-hyperarea vectors for facets of a median-dual region in \mathbb{R}^4 . These geometric properties are key for facilitating the construction of node-centered edge-based schemes in higher dimensions.

2012 ACM Subject Classification Mathematics of computing → Partial differential equations, Theory of computation → Computational geometry

Keywords and phrases Median Dual, Hypervolume, Four dimensions, Space-time, Higher-dimensions

Funding *David M. Williams*: This researcher was funded by the National Institute of Aerospace under grant X-24-801007-PSU

Hiroaki Nishikawa: This researcher was funded by the U.S. Army Research Office under the contract/grant number W911NF-19-1-0429

1 Introduction

Dual tessellations are an important component of node-centered numerical methods. In a node-centered method, the unknowns (degrees of freedom) are the vertices of a triangulation. The dual regions—often called dual control volumes—provide a convenient way to enforce conservation of mass, momentum, or energy in the immediate vicinity of the nodes. The idea of conservation is important in the field of computational fluid dynamics (CFD), as conservation errors can result in incorrect predictions of shockwave speeds and thermodynamic properties [47, 1, 25, 35, 48, 21]. Of course, node-centered numerical methods are not the only methods which enforce conservation; evidently, cell-centered methods accomplish the same task. However, node-centered methods have become increasingly popular due to their exceptional efficiency. For example, *node-centered edge-based* methods have become the foundation of many important CFD codes [4, 2, 39, 30, 37, 34, 29, 24, 49, 16, 17, 22]. These methods are remarkably inexpensive, as they compute the residual using a compact stencil

¹ Distribution Statement A: Approved for public release. Distribution is unlimited.

that only involves the solution and gradients at the current node and its edge-neighbors. Conservation is enforced via careful calculations of numerical fluxes at the dual facets which intersect the edges. In addition, fluxes through dual facets over the boundaries are added with special accuracy-preserving formulas [41, 42]; furthermore, boundary conditions are enforced through an upwind numerical flux with the external state defined by a physical boundary condition [31]. Generally speaking, node-centered, edge-based methods are quite fast, as they only require a single loop over edges in order to compute the residuals, and a single loop over boundary elements to close the residuals at boundary nodes and enforce boundary conditions. Most importantly, node-centered, edge-based methods are capable of achieving second-order or third-order accuracy on unstructured triangulations in 2D [26, 27, 15] and 3D [31, 46]. We note that third-order accuracy can be achieved with a single numerical flux per edge, without requiring quadratic (curved) triangulations [31, 42], or second-derivative information [45].

In principle, a node-centered, edge-based scheme can be employed on *any* dual tessellation, subject to the following geometric constraints:

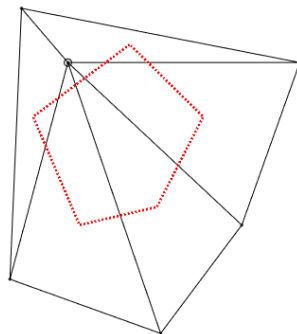
- (a) The dual cell for a given node must contain the node.
- (b) The dual cell must be contained within the union of all d -simplices which share the node.
- (c) The dual cell must be simply connected.
- (d) The aggregate hypervolumes of the dual tessellation and the original triangulation must be identical.

The first two constraints help ensure proximity of the dual cell and the associated node, and sizing (scale) of the dual cell relative to the initial triangulation. The last two constraints help enforce conservation. Of course, most well-known dual tessellations satisfy these constraints. However, *median-dual* tessellations are the most popular. First of all, this is because the existing node-centered edge-based method is second- or third-order accurate only with median-dual tessellations on simplex-element grids, and first-order accurate otherwise (see, e.g. [43]). More generally, there are important reasons based on geometric considerations. These considerations are discussed in more detail below.

1.1 Geometric Background

A median-dual tessellation of a triangulation in \mathbb{R}^d is a set of d -polytopal cells which covers the domain of triangulation, where the vertices of the dual regions are the centroids of 2-simplices, 3-simplices, ..., and d -simplices which belong to the triangulation, and share a given node. The resulting regions are simply connected, possess straight edges, always contain the central node of interest, and are (often) non-convex. By construction, the regions possess the same aggregate hypervolume as the original triangulation. It is important to note that median-dual regions are not (usually) identical to *centroid-dual* regions, see [5]. For example in 2D, centroid-dual regions are formed by connecting the centroids of adjacent 2-simplices (triangles) which share a given node. A line segment connecting the centroids of adjacent 2-simplices rarely crosses the shared edge at the midpoint; therefore, the facet intersection points for the median-dual and centroid-dual regions are often different. Unfortunately, centroid-dual regions violate one of our geometric constraints: namely, they can fail to contain the central node of interest. Figure 1 shows an example of this issue.

With the above discussion in mind, it makes sense to consider developing dual tessellations based on non-centroidal quantities, such as incenters, hypercircumcenters, or orthocenters. Each of these geometric quantities generalize to higher dimensions, $d \geq 4$. Unfortunately, some of these alternative options violate our geometric constraints. For example, the hypercircumcenters and orthocenters of d -simplices are not guaranteed to reside within



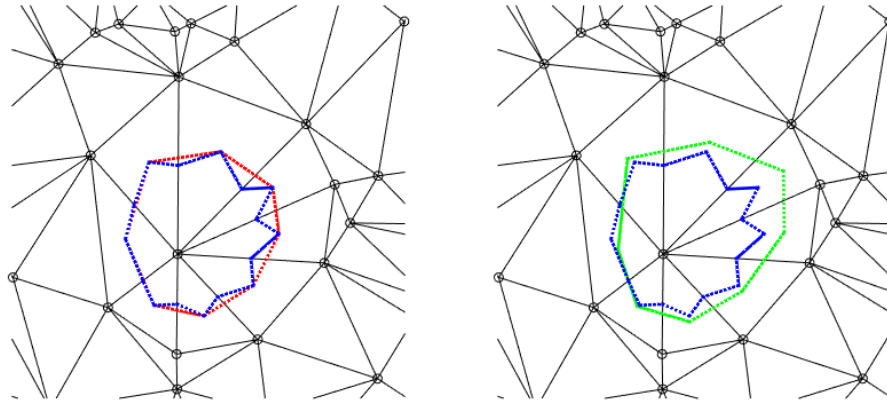
■ **Figure 1** An example of the centroid-dual region not containing the associated node in 2D. The associated node is denoted by an open circle, and the region is denoted with a dotted-red line.

the interiors of the simplices. Even in 2D, the circumcenter and orthocenter of an obtuse 2-simplex lie outside of the simplex [14]. Fortunately, by construction, the incenter lies inside of the d -simplex. However, the computation of the incenter for a d -simplex often requires the solution of a linear system of equations, (see for example [28]). It is unclear that one gains any advantage from this additional complexity.

Our discussion of dual tessellations would be incomplete without mentioning *Voronoi* and *Laguerre* tessellations. The Voronoi tessellation (or Voronoi diagram) [51, 50], is a space-efficient subdivision of a domain, in which each dual cell contains all the points in the domain which are closer to the central node of the cell than they are to any other node in the triangulation. The Voronoi dual cells are convex, simply connected, and possess straight edges. It is well-known that Voronoi tessellations are the duals of Delaunay triangulations—assuming all the points of the Voronoi cells are in general position [8]. In a similar fashion, a Laguerre tessellation (or Power diagram) [7, 3] is the dual of a weighted-Delaunay triangulation [8]. The nodes of a weighted-Delaunay triangulation can be treated like hyperspheres with different radii that depend on the weights; in turn, the Laguerre dual cell for a given hypersphere contains all the points which are closer to the central hypersphere than they are to any other hypersphere in the weighted triangulation. Unfortunately, most algorithms which construct Voronoi or Laguerre tessellations must start with a Delaunay or weighted-Delaunay triangulation algorithm [9, 52], (with the exception of Fortune’s algorithm [18]). This inhibits the use of these tessellations for non-Delaunay triangulations.

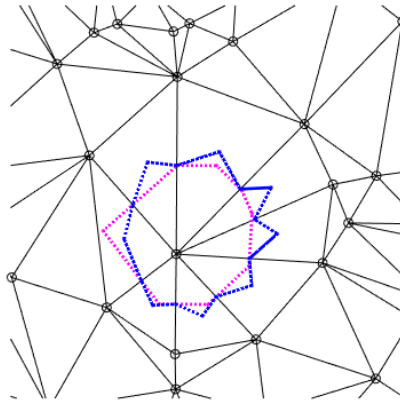
For the sake of completeness, Figures 2 and 3 highlight the differences between median-dual, centroid-dual, incenter-dual, and Voronoi regions on a 2D Delaunay triangulation.

In summary, the key advantages of a median-dual tessellation are flexibility and simplicity. In particular, a median-dual tessellation can be formed based on *any* valid triangulation of a domain in \mathbb{R}^d , without requiring the solutions of linear systems. This does not generally hold true for centroid-dual, incenter-dual, Voronoi, or Laguerre tessellations, or variants thereof. We note that flexibility is especially important, as there are many alternative strategies for building triangulations in \mathbb{R}^d , including the advancing-front approach [33, 23, 38, 12, 32], and the hybrid Delaunay/advancing-front approach [36, 20]. In addition, even if the original triangulation of interest satisfies the Delaunay criterion, it is often necessary to adaptively refine the triangulation in order to resolve important features of the solution [40, 11, 10, 6]. Generally speaking, the Delaunay criterion is not satisfied after this adaptive process is



(a) Median-dual and centroid-dual.

(b) Median-dual and incenter-dual.



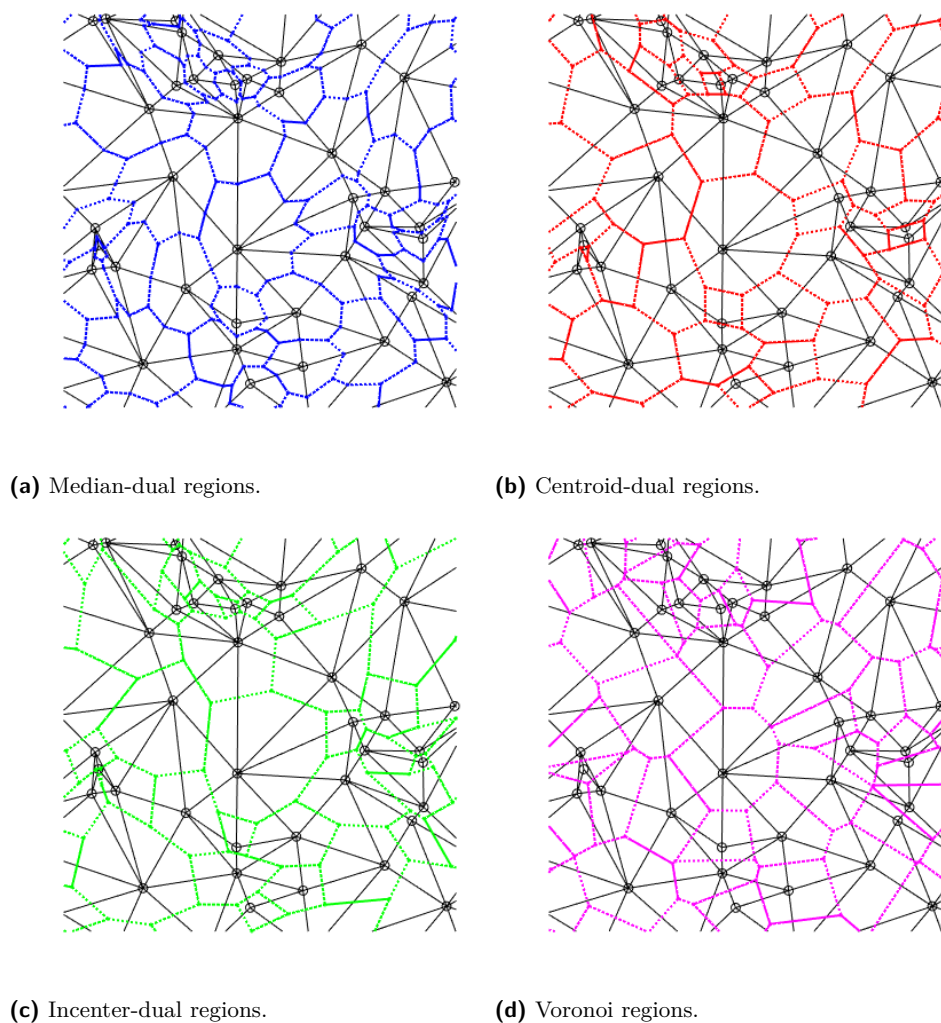
(c) Median-dual and Voronoi.

■ **Figure 2** An illustration comparing the median-dual region (dotted-blue line) to the centroid-dual region (dotted-red line, subfigure a), incenter-dual region (dotted-green line, subfigure b), and Voronoi region (dotted-magenta line, subfigure c) for a generic node of a Delaunay triangulation in 2D.

complete. As a result, we require dual tessellation strategies that are capable of operating on generic triangulations which emerge from such processes.

1.2 Recent Developments

In previous years, CFD practitioners have often implemented node-centered, edge-based methods by *explicitly* constructing median-dual regions (e.g. median-dual vertices, edges, faces, and volumes in 2D or 3D). However, Nishikawa [44] recently discovered that this is unnecessary. Rather, it is possible to develop a node-centered scheme which only requires certain geometric properties of the median-dual regions: namely, the hypervolumes of the dual regions, as well as the directed-hyperarea vectors associated with the edges [44]. In 3D, the directed-hyperarea vectors are area-weighted vectors which point from the current node towards neighboring nodes. Furthermore, the area weighting is associated with the area of the



■ **Figure 3** An illustration showing the median-dual regions (dotted-blue lines), centroid-dual regions (dotted-red lines), incenter-dual regions (dotted-green lines), and Voronoi regions (dotted-magenta lines) for multiple nodes, on a Delaunay triangulation in 2D.

dual face through which each edge crosses. With these definitions established, it is desirable to identify algebraic formulas for computing the dual hypervolume and directed-hyperarea vectors, which are entirely based on geometric properties of the d -simplices which share a given node. This avoids the complex task of explicitly constructing the median-dual regions, and then extracting the necessary geometric quantities. In 2D and 3D, Nishikawa has recently obtained the desired formulas [44], and demonstrated their correctness. However, it remains for us to extend these formulas to 4D (and higher dimensions), and rigorously prove their correctness in this new context.

1.3 Overview of the Paper

In this work, we construct a precise definition for median-dual regions in \mathbb{R}^d . In addition, we develop explicit formulas for the hypervolumes and directed-hyperarea vectors of these median-dual regions. We prove that our formula for the dual hypervolume holds in any

number of dimensions. Furthermore, we prove that the directed-hyperarea formula holds in 4D.

The format of the paper is as follows. In section 2 we introduce preliminary geometric concepts and define the median-dual region in \mathbb{R}^d . In section 3 we prove an explicit hypervolume formula in \mathbb{R}^d . Next, in section 4 we prove an explicit directed-hyperarea formula in \mathbb{R}^4 , and discuss implementation and verification procedures. Finally, in section 5 we present some concluding remarks.

2 Preliminaries

Consider a set of distinct points in general position

$$\mathcal{P} = \{\mathbf{p}_1, \mathbf{p}_2, \dots, \mathbf{p}_\ell, \dots, \mathbf{p}_L\}, \quad (1)$$

where L is the total number of points, and $1 \leq \ell \leq L$. Now, suppose that we are interested in forming a triangulation of \mathcal{P} . Towards this end, let us define a domain $\Omega = \text{conv}(\mathcal{P})$. A valid triangulation \mathcal{T} of the domain Ω is one which covers Ω with non-overlapping d -simplicial elements, such that the sum of the hypervolumes of the elements is identical to the hypervolume of Ω itself. In more technical terms, \mathcal{T} is a *pseudo manifold*, i.e. a pure simplicial d -complex that is d -connected, and for which each $(d-1)$ -face has at most one or two d -simplicial neighbors. Such a triangulation can be formed in a straightforward fashion by using one of the techniques previously mentioned in the Introduction.

For the sake of completeness, let us denote $T^{(d)}$ as the generic d -simplex that belongs to \mathcal{T} . This simplex is the convex hull of $d+1$ points

$$\begin{aligned} T = T^{(d)} &= \text{conv}(\mathbf{p}_{T,1}, \mathbf{p}_{T,2}, \dots, \mathbf{p}_{T,n}, \dots, \mathbf{p}_{T,d+1}), \\ &= \text{conv}(\mathbf{p}_{i_1}, \mathbf{p}_{i_2}, \dots, \mathbf{p}_{i_n}, \dots, \mathbf{p}_{i_{d+1}}), \end{aligned} \quad (2)$$

where $1 \leq n \leq (d+1)$. We omit the superscript (d) when our meaning is clear. In Eq. (2), the quantity $\mathbf{p}_{T,n}$ is a point labeled with the *local numbering* of simplex $T^{(d)}$, and the quantity \mathbf{p}_{i_n} is the same point labeled with the *global numbering* of set \mathcal{P} .

Once each element $T^{(d)}$ has been constructed, we can define the appropriate *median* quantities, as follows.

2.1 Vertex-Based Quantities

We start by introducing the set of all edges in the mesh that start at point \mathbf{p}_j and end at adjacent points $\mathbf{p}_1, \mathbf{p}_2, \dots, \mathbf{p}_k, \dots, \mathbf{p}_{M_1}$

$$\begin{aligned} \mathbb{T}_j^{(1)} &\equiv \{\mathbf{p}_1 - \mathbf{p}_j, \mathbf{p}_2 - \mathbf{p}_j, \dots, \mathbf{p}_k - \mathbf{p}_j, \dots, \mathbf{p}_{M_1} - \mathbf{p}_j\} \\ &= \{T_{j,1}^{(1)}, T_{j,2}^{(1)}, \dots, T_{j,k}^{(1)}, \dots, T_{j,M_1}^{(1)}\}, \end{aligned} \quad (3)$$

where $1 \leq k \leq M_1$ and $M_1 = |\mathbb{T}_j^{(1)}|$ is the total number of points which are adjacent (edge-wise) to \mathbf{p}_j . In addition, we can denote the centroid of each edge as follows

$$\begin{aligned} \mathcal{C}_j^{(1)} &\equiv \frac{1}{2} \{\mathbf{p}_1 + \mathbf{p}_j, \mathbf{p}_2 + \mathbf{p}_j, \dots, \mathbf{p}_k + \mathbf{p}_j, \dots, \mathbf{p}_{M_1} + \mathbf{p}_j\} \\ &= \{\mathbf{c}_{j,1}^{(1)}, \mathbf{c}_{j,2}^{(1)}, \dots, \mathbf{c}_{j,k}^{(1)}, \dots, \mathbf{c}_{j,M_1}^{(1)}\}. \end{aligned} \quad (4)$$

Next, we introduce the set of triangles (2-simplices) that contain the point \mathbf{p}_j

$$\mathbb{T}_j^{(2)} \equiv \left\{ T_{j,1}^{(2)}, T_{j,2}^{(2)}, \dots, T_{j,k}^{(2)}, \dots, T_{j,M_2}^{(2)} \right\}, \quad (5)$$

along with their centroids

$$\mathcal{C}_j^{(2)} \equiv \left\{ \mathbf{c}_{j,1}^{(2)}, \mathbf{c}_{j,2}^{(2)}, \dots, \mathbf{c}_{j,k}^{(2)}, \dots, \mathbf{c}_{j,M_2}^{(2)} \right\}, \quad (6)$$

where $1 \leq k \leq M_2$ and $M_2 = \left| \mathbb{T}_j^{(2)} \right|$. More generally, we introduce the set of q -simplices which share the point \mathbf{p}_j

$$\mathbb{T}_j^{(q)} \equiv \left\{ T_{j,1}^{(q)}, T_{j,2}^{(q)}, \dots, T_{j,k}^{(q)}, \dots, T_{j,M_q}^{(q)} \right\}, \quad (7)$$

along with their centroids

$$\mathcal{C}_j^{(q)} \equiv \left\{ \mathbf{c}_{j,1}^{(q)}, \mathbf{c}_{j,2}^{(q)}, \dots, \mathbf{c}_{j,k}^{(q)}, \dots, \mathbf{c}_{j,M_q}^{(q)} \right\}, \quad (8)$$

where $1 \leq k \leq M_q$, $M_q = \left| \mathbb{T}_j^{(q)} \right|$, and $1 \leq q \leq d$.

We have introduced all of the relevant vertex-based quantities (see above). These quantities have been partitioned into convenient sets, denoted by (for example) $\mathbb{T}_j^{(q)}$ and $\mathcal{C}_j^{(q)}$. In a natural fashion, we can also construct larger sets, which are based on the *power set* of the smaller sets. In particular, we can define the supersets of all simplices and centroids that share the point \mathbf{p}_j as follows

$$\mathbb{T}_j \equiv \left\{ \mathbb{T}_j^{(1)}, \mathbb{T}_j^{(2)}, \dots, \mathbb{T}_j^{(q)}, \dots, \mathbb{T}_j^{(d)} \right\}, \quad \mathcal{C}_j \equiv \left\{ \mathcal{C}_j^{(1)}, \mathcal{C}_j^{(2)}, \dots, \mathcal{C}_j^{(q)}, \dots, \mathcal{C}_j^{(d)} \right\}. \quad (9)$$

2.2 Median-Dual Definitions

We are now ready to formulate the definition of the median-dual region.

► **Definition 1** (Median-Dual Region). *Consider a point \mathbf{p}_j in a d -simplicial triangulation. We can form the median-dual region for \mathbf{p}_j by taking the union of the convex hulls of the centroids (in the superset \mathcal{C}_j) which belong to each d -simplex $T_{j,k}^{(d)}$, where each simplex shares the vertex \mathbf{p}_j and $1 \leq k \leq M_d$. Equivalently, the median-dual region (MDR) around \mathbf{p}_j is given by the following*

$$\text{MDR}(\mathbf{p}_j) = \bigcup_{k=1}^{M_d} \text{conv} \left(\mathbf{c} \in \left(\mathcal{C}_j \cap T_{j,k}^{(d)} \right) \right), \quad (10)$$

where \mathbf{c} is a generic centroid that belongs to the intersection of \mathcal{C}_j and $T_{j,k}^{(d)} \in \mathbb{T}_j^{(d)}$.

We can now introduce a very rudimentary formula for the hypervolume of each median-dual region. This result is required in order to develop a subsequent, more sophisticated hypervolume identity (see Theorem 5).

► **Lemma 2** (Median-Dual Hypervolume). *The hypervolume of the median-dual region around \mathbf{p}_j is given by the following formula*

$$V(\mathbf{p}_j) = \frac{1}{d+1} \sum_{k=1}^{M_d} \left| T_{j,k}^{(d)} \right|, \quad (11)$$

where $T_{j,k}^{(d)} \in \mathbb{T}_j^{(d)}$ is a d -simplex that shares the node \mathbf{p}_j .

Proof. By construction, the median dual region covers exactly $1/(d+1)$ th of each d -simplex which contains the node \mathbf{p}_j . The summation of these partial hypervolume contributions from each $T_{j,k}^{(d)}$ yields the total hypervolume of the region. ◀

2.3 Edge-Based Quantities

We can define the set of all q -simplices which share the edge $\mathbf{p}_k - \mathbf{p}_j$

$$\mathbb{T}_{jk}^{(q)} \equiv \left\{ T_{jk,1}^{(q)}, T_{jk,2}^{(q)}, \dots, T_{jk,v}^{(q)}, \dots, T_{jk,N_q}^{(q)} \right\},$$

where $1 \leq v \leq N_q$ and $N_q = |\mathbb{T}_{jk}^{(q)}|$. The centroids of the q -simplices are given by

$$\mathcal{C}_{jk}^{(q)} \equiv \left\{ \mathbf{c}_{jk,1}^{(q)}, \mathbf{c}_{jk,2}^{(q)}, \dots, \mathbf{c}_{jk,v}^{(q)}, \dots, \mathbf{c}_{jk,N_q}^{(q)} \right\}.$$

The supersets of *all* simplices and centroids ($q = 1, \dots, d$) which share the edge $\mathbf{p}_k - \mathbf{p}_j$ are given by

$$\mathbb{T}_{jk} = \left\{ \mathbb{T}_{jk}^{(1)}, \mathbb{T}_{jk}^{(2)}, \dots, \mathbb{T}_{jk}^{(q)}, \dots, \mathbb{T}_{jk}^{(d)} \right\}, \quad \mathcal{C}_{jk} = \left\{ \mathcal{C}_{jk}^{(1)}, \mathcal{C}_{jk}^{(2)}, \dots, \mathcal{C}_{jk}^{(q)}, \dots, \mathcal{C}_{jk}^{(d)} \right\}.$$

2.4 Directed-Hyperarea Vector Definition

► **Definition 3** (Directed-Hyperarea Vectors). *Consider a point \mathbf{p}_j in a d -simplicial triangulation. The directed-hyperarea vectors for this point are vectors which are aligned with each edge emanating from the point. More precisely, the vectors themselves are denoted by*

$$\{\mathbf{n}_{j1}, \mathbf{n}_{j2}, \dots, \mathbf{n}_{jk}, \dots, \mathbf{n}_{jM_1}\}, \quad (12)$$

and are aligned with edges

$$\{\mathbf{p}_1 - \mathbf{p}_j, \mathbf{p}_2 - \mathbf{p}_j, \dots, \mathbf{p}_k - \mathbf{p}_j, \dots, \mathbf{p}_{M_1} - \mathbf{p}_j\}.$$

Furthermore

$$\mathbf{n}_{jk} \equiv \sum_{T \in \{\mathbb{T}_{jk}^{(d)}\}} \mathbf{n}(T), \quad (13)$$

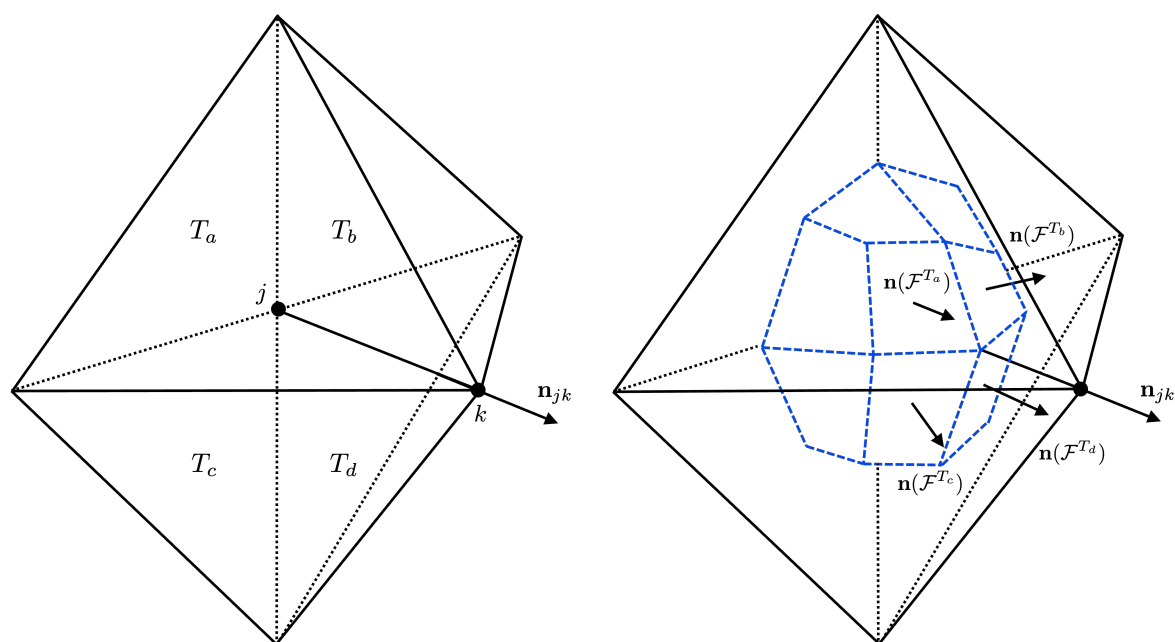
where $\mathbf{n}(T)$ is the lumped-normal vector of the $(d-1)$ -hypercube facet that is constructed from centroids which are contained in each T ; (see Figures 4 and 5 for an illustration of the quantities in the formula). More precisely, the lumped-normal vector of a hypercube is defined as the unique sum of the normal vectors of a simplicial tessellation of the hypercube. For example, it is the sum of the normal vectors of two triangles which make up a quadrilateral. Moreover, each hypercube facet is given by

$$\mathcal{F}^T \equiv \text{conv}(\mathbf{c} \in (\mathcal{C}_{jk} \cap T)), \quad (14)$$

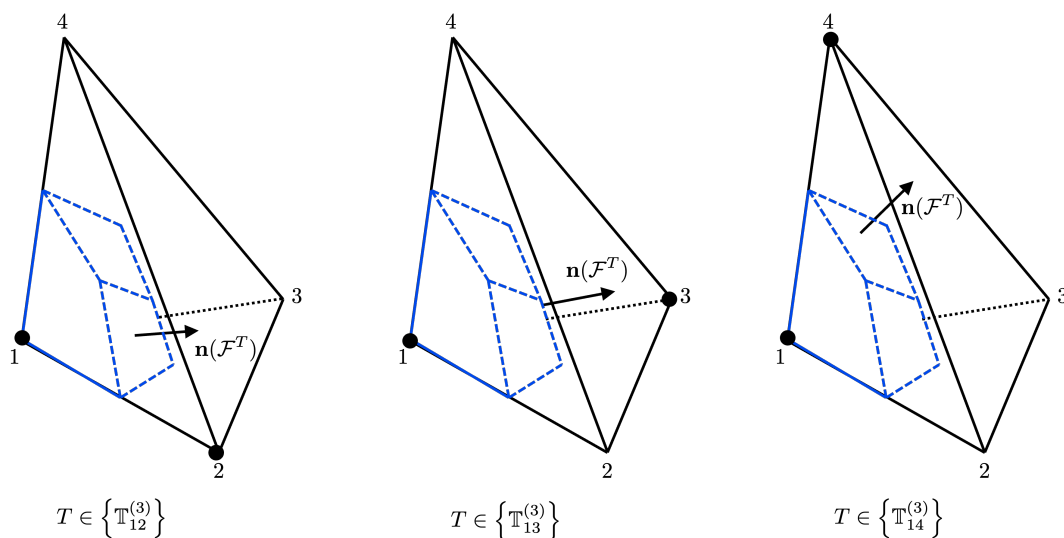
where \mathbf{c} is a generic centroid that belongs to the intersection of the superset \mathcal{C}_{jk} and T , and T is a generic d -simplex that belongs to

$$\mathbb{T}_{jk}^{(d)} \equiv \left\{ T_{jk,1}^{(d)}, T_{jk,2}^{(d)}, \dots, T_{jk,v}^{(d)}, \dots, T_{jk,N_d}^{(d)} \right\}.$$

Here, $\mathbb{T}_{jk}^{(d)}$ is the set of d -simplices that share the edge $\mathbf{p}_k - \mathbf{p}_j$.



■ **Figure 4** A 3D illustration of a directed-hyperarea vector \mathbf{n}_{jk} for the edge $\mathbf{p}_k - \mathbf{p}_j$ (left). The edge is shared by four tetrahedra T_a, T_b, T_c and T_d . The lumped-normal vectors of the dual hypercuboid facets are summed together in order to obtain \mathbf{n}_{jk} (right). More precisely, $\mathbf{n}_{jk} = \mathbf{n}(\mathcal{F}^{T_a}) + \mathbf{n}(\mathcal{F}^{T_b}) + \mathbf{n}(\mathcal{F}^{T_c}) + \mathbf{n}(\mathcal{F}^{T_d})$. The (partial) median-dual region around node \mathbf{p}_j is highlighted in blue.



■ **Figure 5** A 3D illustration of the lumped-normal vector of the hypercuboid facet $\mathbf{n}(\mathcal{F}^T)$ which contributes to directed-hyperarea vector \mathbf{n}_{12} (left). The lumped-normal vector $\mathbf{n}(\mathcal{F}^T)$ which contributes to \mathbf{n}_{13} (center). The lumped-normal vector $\mathbf{n}(\mathcal{F}^T)$ which contributes to \mathbf{n}_{14} (right). These lumped-normal vectors are shown for a generic tetrahedron T which belongs to $\mathbb{T}_{12}^{(3)}, \mathbb{T}_{13}^{(3)}$, and $\mathbb{T}_{14}^{(3)}$. The (partial) median-dual region around node \mathbf{p}_1 is highlighted in blue.

3 Theoretical Properties in \mathbb{R}^d

In this section, we establish important theoretical properties and conjectures which govern median-dual regions in \mathbb{R}^d .

► **Conjecture 4** (Directed-Hyperarea Vector Identity in \mathbb{R}^d). *Suppose that we construct a median-dual region around an interior point $\mathbf{p}_j \in \mathbb{R}^d$. In addition, let a generic adjacent edge be denoted by $\mathbf{p}_k - \mathbf{p}_j$. Under these circumstances, the following identity holds*

$$\mathbf{n}_{jk} = \frac{2}{d(d+1)} \sum_{T \in \{\mathbb{T}_{jk}^{(d)}\}} \mathbf{n}_j^T, \quad (15)$$

where \mathbf{n}_j^T is a normal vector associated with the $(d-1)$ -facet of T opposite j . We note that \mathbf{n}_j^T has a magnitude which is equal to the hypervolume of the opposite facet, i.e. $\|\mathbf{n}_j^T\| = |\text{opp}_j(T)|$.

Proof. We are unaware of a proof for this conjecture for $d > 4$. However, the cases of $d = 2$ and 3 were proven in [44]. In addition, the case of $d = 4$ can be proven using careful arguments, see Theorem 6 of the present paper. ◀

► **Theorem 5** (Hypervolume Identity in \mathbb{R}^d). *The following relationship between the hypervolume of the median-dual region $V(\mathbf{p}_j)$ and the directed-hyperarea vectors \mathbf{n}_{jk} holds*

$$\begin{aligned} V(\mathbf{p}_j) &= \frac{1}{d^2(d+1)} \sum_{k=1}^{M_1} \left(\sum_{T \in \{\mathbb{T}_{jk}^{(d)}\}} (\mathbf{p}_k - \mathbf{p}_j) \cdot \mathbf{n}_j^T \right) \\ &= \frac{1}{2d} \sum_{k=1}^{M_1} (\mathbf{p}_k - \mathbf{p}_j) \cdot \mathbf{n}_{jk}, \end{aligned} \quad (16)$$

where the second line follows from Conjecture 4.

Proof. Our objective is to prove that Eqs. (11) and (16) are equivalent. Towards this end, let us consider the *altitude* h_j^T of the facet opposite \mathbf{p}_j for each $T \in \{\mathbb{T}_{jk}^{(d)}\}$, which is given by

$$h_j^T \equiv (\mathbf{p}_k - \mathbf{p}_j) \cdot \frac{\mathbf{n}_j^T}{\|\mathbf{n}_j^T\|}, \quad (17)$$

where $\|\mathbf{n}_j^T\|$ is the hypervolume of the facet opposite \mathbf{p}_j . Upon substituting Eq. (17) into the first line of Eq. (16), we obtain

$$V(\mathbf{p}_j) = \frac{1}{d^2(d+1)} \sum_{k=1}^{M_1} \left(\sum_{T \in \{\mathbb{T}_{jk}^{(d)}\}} h_j^T \|\mathbf{n}_j^T\| \right). \quad (18)$$

Furthermore, the hypervolume of each d -simplex $T \in \{\mathbb{T}_{jk}^{(d)}\}$ is given by

$$|T| = \frac{h_j^T}{d} \|\mathbf{n}_j^T\|. \quad (19)$$

Substituting Eq. (19) into Eq. (18) yields

$$V(\mathbf{p}_j) = \frac{1}{d(d+1)} \sum_{k=1}^{M_1} \left(\sum_{T \in \{\mathbb{T}_{jk}^{(d)}\}} |T| \right). \quad (20)$$

Now, we must compare our newly obtained expression, Eq. (20), to our previously obtained expression for the median-dual hypervolume, Eq. (11). If these equations are identical, then we can immediately conclude that our desired result, Eq. (16), holds. Upon attempting to equate Eqs. (20) and (11), we require that

$$\begin{aligned} \frac{1}{d} \sum_{k=1}^{M_1} \left(\sum_{T \in \{\mathbb{T}_{jk}^{(d)}\}} |T| \right) &= \sum_{m=1}^{M_d} |T_{j,m}^{(d)}| \\ &= \sum_{T \in \{\mathbb{T}_j^{(d)}\}} |T|. \end{aligned} \quad (21)$$

Careful analysis reveals that the equality in Eq. (21) is correct. By inspection, the left hand side of the equation is a weighted summation over the d -simplices that share the edges $\mathbf{p}_k - \mathbf{p}_j$, and the right hand side is a summation over the d -simplices which share the point \mathbf{p}_j . Evidently, the left hand side and right hand side of our equation contain the *same* simplices, as all simplices which share the point \mathbf{p}_j also contain exactly d edges $\mathbf{p}_k - \mathbf{p}_j$. In fact, it is impossible for a d -simplex to contain the point \mathbf{p}_j , but fail to contain d of the edges $\mathbf{p}_k - \mathbf{p}_j$ which emanate from it. This observation follows from the definition of a d -simplex in \mathbb{R}^d , as each point of the simplex is connected via edges to d other points of the same simplex. In addition, we note that the summation over edges on the left hand side of our equation must be normalized by a factor of $(1/d)$ in order to account for the fact that each simplex hypervolume $|T|$ contributes to the summation d times, as it is shared by d edges which connect to \mathbf{p}_j , (as mentioned previously). This final observation completes the proof. ◀

4 Theoretical Properties in \mathbb{R}^4

In this section, we establish an important theoretical property which governs median-dual regions in \mathbb{R}^4 , along with several key implementation and verification details.

► **Theorem 6** (Directed-Hyperarea Vector Identity in \mathbb{R}^4). *Suppose that we construct a median-dual region around an interior point $\mathbf{p}_j \in \mathbb{R}^4$. In addition, let a generic adjacent edge be denoted by $\mathbf{p}_k - \mathbf{p}_j$. Under these circumstances, the following identity holds*

$$\mathbf{n}_{jk} = \frac{1}{10} \sum_{T \in \{\mathbb{T}_{jk}^{(4)}\}} \mathbf{n}_j^T, \quad (22)$$

where \mathbf{n}_j^T is a normal vector associated with the 3-facet of T opposite j . We note that \mathbf{n}_j^T has a magnitude which is equal to the hypervolume of the opposite facet, i.e. $\|\mathbf{n}_j^T\| = |\text{opp}_j(T)|$.

Proof. We start by introducing a generic edge $\mathbf{p}_2 - \mathbf{p}_1$ which connects points $\mathbf{p}_1 \in \mathbb{R}^4$ and $\mathbf{p}_2 \in \mathbb{R}^4$. For the sake of this proof, we are interested in computing the directed-hyperarea vector \mathbf{n}_{12} , and showing that the left hand side of Eq. (22) is equivalent to the right hand side, for this case. Towards this end, we assume that the edge $\mathbf{p}_2 - \mathbf{p}_1$ is shared by a total

12 Median-Dual Regions on Triangulations in \mathbb{R}^d

of N_4 pentatopes (4-simplices), where $N_4 = |\mathbb{T}_{12}^{(4)}|$. Let us consider a single one of these 4-simplices

$$T_\alpha = \text{conv}(\{\mathbf{p}_1, \mathbf{p}_2, \mathbf{p}_3, \mathbf{p}_4, \mathbf{p}_5\}), \quad T_\alpha \in \mathbb{T}_{12}^{(4)}. \quad (23)$$

In a natural fashion, the simplex T_α contributes to our calculation of \mathbf{n}_{12} . In particular, in accordance with the definition of our directed-hyperarea vector, (see Eq. (13)), we find that

$$\mathbf{n}_{12} = \sum_{T \in \{\mathbb{T}_{12}^{(4)}\}} \mathbf{n}(\mathcal{F}^T), \quad (24)$$

where

$$\mathcal{F}^T = \text{conv}(\mathbf{c} \in (\mathcal{C}_{12} \cap T)). \quad (25)$$

Naturally, the contribution from T_α to Eq. (24) appears to be given by $\mathbf{n}(\mathcal{F}^{T_\alpha})$. However, this is not the complete truth, as some of the contributions to \mathbf{n}_{12} from T_α will be canceled by its neighbors. In order to avoid overlooking these cancellations, we must simultaneously compute the contributions to \mathbf{n}_{12} from T_α and its 3-facet neighbors. With this in mind, let us define the three, 3-facet neighbors of T_α as follows

$$T_\beta = \text{conv}(\{\mathbf{p}_1, \mathbf{p}_2, \mathbf{p}_3, \mathbf{p}_4, \mathbf{p}_6\}), \quad (26)$$

$$T_\gamma = \text{conv}(\{\mathbf{p}_1, \mathbf{p}_2, \mathbf{p}_3, \mathbf{p}_5, \mathbf{p}_7\}), \quad (27)$$

$$T_\delta = \text{conv}(\{\mathbf{p}_1, \mathbf{p}_2, \mathbf{p}_4, \mathbf{p}_5, \mathbf{p}_8\}), \quad (28)$$

where $T_\beta, T_\gamma, T_\delta \in \mathbb{T}_{12}^{(4)}$. Figure 6 shows an illustration of T_α and its facet neighbors T_β, T_γ , and T_δ .

We can now compute the individual contributions $\mathbf{n}(\mathcal{F}^{T_\alpha})$, $\mathbf{n}(\mathcal{F}^{T_\beta})$, $\mathbf{n}(\mathcal{F}^{T_\gamma})$, and $\mathbf{n}(\mathcal{F}^{T_\delta})$. These lumped-normal vectors are computed based on the median quantities associated with each d -simplex. Let us begin by computing the relevant median quantities for T_α . The centroids $\mathbf{c} \in (\mathcal{C}_{12} \cap T_\alpha)$ are given by

$$\mathbf{c}_a = \frac{1}{2}(\mathbf{p}_1 + \mathbf{p}_2), \quad (29)$$

$$\mathbf{c}_b = \frac{1}{3}(\mathbf{p}_1 + \mathbf{p}_2 + \mathbf{p}_3), \quad (30)$$

$$\mathbf{c}_c = \frac{1}{3}(\mathbf{p}_1 + \mathbf{p}_2 + \mathbf{p}_4), \quad (31)$$

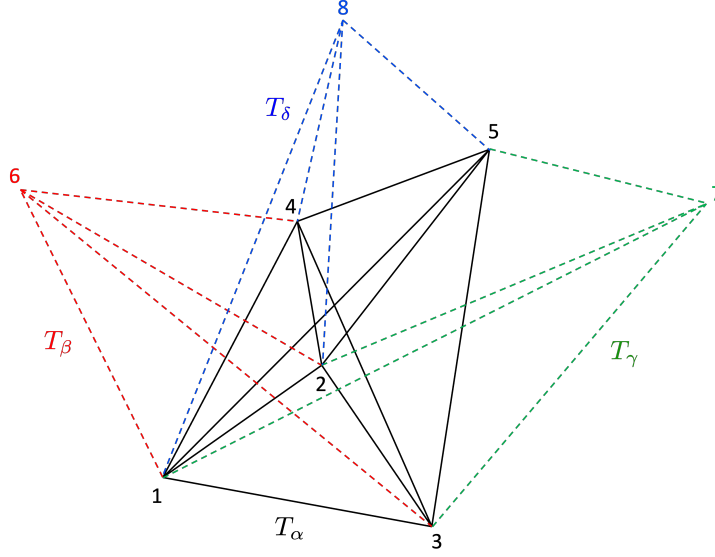
$$\mathbf{c}_d = \frac{1}{3}(\mathbf{p}_1 + \mathbf{p}_2 + \mathbf{p}_5), \quad (32)$$

$$\mathbf{c}_e = \frac{1}{4}(\mathbf{p}_1 + \mathbf{p}_2 + \mathbf{p}_3 + \mathbf{p}_4), \quad (33)$$

$$\mathbf{c}_f = \frac{1}{4}(\mathbf{p}_1 + \mathbf{p}_2 + \mathbf{p}_4 + \mathbf{p}_5), \quad (34)$$

$$\mathbf{c}_g = \frac{1}{4}(\mathbf{p}_1 + \mathbf{p}_2 + \mathbf{p}_3 + \mathbf{p}_5), \quad (35)$$

$$\mathbf{c}_h = \frac{1}{5}(\mathbf{p}_1 + \mathbf{p}_2 + \mathbf{p}_3 + \mathbf{p}_4 + \mathbf{p}_5). \quad (36)$$



■ **Figure 6** An illustration of the 4-simplex T_α and its three facet neighbors. The simplex T_α is drawn with solid black lines. The neighboring simplices are drawn with dashed lines; in particular, T_β is drawn with dashed red lines, T_γ is drawn with dashed green lines, and T_δ is drawn with dashed blue lines.

These centroids form a 3-cuboid with eight vertices. We denote this cuboid by \mathcal{F}^{T_α} , where

$$\mathcal{F}^{T_\alpha} = \text{conv}(\mathbf{c} \in (\mathcal{C}_{12} \cap T_\alpha)) = \text{conv}(\{\mathbf{c}_a, \mathbf{c}_b, \mathbf{c}_c, \mathbf{c}_d, \mathbf{c}_e, \mathbf{c}_f, \mathbf{c}_g, \mathbf{c}_h\}). \quad (37)$$

Computing the lumped-normal vector of the cuboid, $\mathbf{n}(\mathcal{F}^{T_\alpha})$, is relatively straightforward. We simply compute the Coxeter–Freudenthal–Kuhn [13, 19] (CFK) triangulation of the cuboid, and then aggregate (sum over) the normal vectors of the resulting 3-simplices. These 3-simplices are given by

$$T_A^{(3)} = \text{conv}(\{\mathbf{c}_a, \mathbf{c}_b, \mathbf{c}_d, \mathbf{c}_e\}), \quad T_B^{(3)} = \text{conv}(\{\mathbf{c}_a, \mathbf{c}_c, \mathbf{c}_d, \mathbf{c}_e\}), \quad (38)$$

$$T_C^{(3)} = \text{conv}(\{\mathbf{c}_c, \mathbf{c}_d, \mathbf{c}_e, \mathbf{c}_f\}), \quad T_D^{(3)} = \text{conv}(\{\mathbf{c}_b, \mathbf{c}_d, \mathbf{c}_e, \mathbf{c}_g\}), \quad (39)$$

$$T_E^{(3)} = \text{conv}(\{\mathbf{c}_e, \mathbf{c}_d, \mathbf{c}_g, \mathbf{c}_h\}), \quad T_F^{(3)} = \text{conv}(\{\mathbf{c}_d, \mathbf{c}_e, \mathbf{c}_f, \mathbf{c}_h\}). \quad (40)$$

Figure 7 shows an illustration of the cuboid, and the associated CFK triangulation.

The spanning vectors for the 3-simplices are given by

$$T_A^{(3)} : \mathbf{v}_{ba} = \mathbf{c}_a - \mathbf{c}_b, \quad \mathbf{v}_{bd} = \mathbf{c}_d - \mathbf{c}_b, \quad \mathbf{v}_{be} = \mathbf{c}_e - \mathbf{c}_b, \quad (41)$$

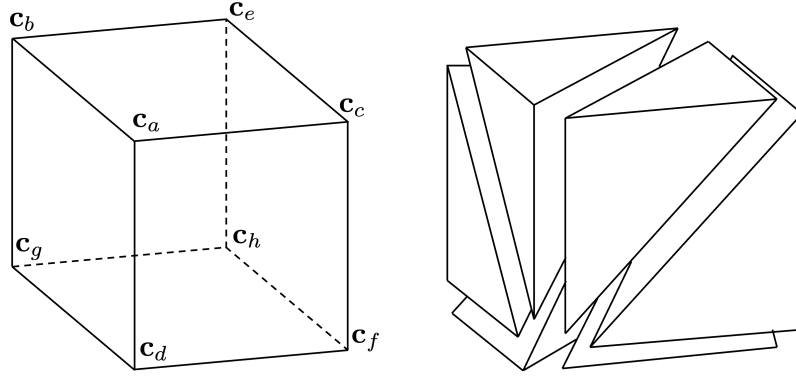
$$T_B^{(3)} : \mathbf{v}_{ce} = \mathbf{c}_e - \mathbf{c}_c, \quad \mathbf{v}_{ca} = \mathbf{c}_a - \mathbf{c}_c, \quad \mathbf{v}_{cd} = \mathbf{c}_d - \mathbf{c}_c, \quad (42)$$

$$T_C^{(3)} : \mathbf{v}_{ce} = \mathbf{c}_e - \mathbf{c}_c, \quad \mathbf{v}_{cd} = \mathbf{c}_d - \mathbf{c}_c, \quad \mathbf{v}_{cf} = \mathbf{c}_f - \mathbf{c}_c, \quad (43)$$

$$T_D^{(3)} : \mathbf{v}_{be} = \mathbf{c}_e - \mathbf{c}_b, \quad \mathbf{v}_{bd} = \mathbf{c}_d - \mathbf{c}_b, \quad \mathbf{v}_{bg} = \mathbf{c}_g - \mathbf{c}_b, \quad (44)$$

$$T_E^{(3)} : \mathbf{v}_{gh} = \mathbf{c}_h - \mathbf{c}_g, \quad \mathbf{v}_{ge} = \mathbf{c}_e - \mathbf{c}_g, \quad \mathbf{v}_{gd} = \mathbf{c}_d - \mathbf{c}_g, \quad (45)$$

$$T_F^{(3)} : \mathbf{v}_{fh} = \mathbf{c}_h - \mathbf{c}_f, \quad \mathbf{v}_{fd} = \mathbf{c}_d - \mathbf{c}_f, \quad \mathbf{v}_{fe} = \mathbf{c}_e - \mathbf{c}_f. \quad (46)$$



■ **Figure 7** An idealized illustration of the cuboid \mathcal{F}^{T_α} (left). The Coxeter-Freudenthal-Kuhn triangulation of the cuboid (right).

The associated normal vectors are

$$T_A^{(3)} : \frac{1}{6} \mathbf{v}_{ba} \times \mathbf{v}_{bd} \times \mathbf{v}_{be}, \quad T_B^{(3)} : \frac{1}{6} \mathbf{v}_{ce} \times \mathbf{v}_{ca} \times \mathbf{v}_{cd}, \quad (47)$$

$$T_C^{(3)} : \frac{1}{6} \mathbf{v}_{ce} \times \mathbf{v}_{cd} \times \mathbf{v}_{cf}, \quad T_D^{(3)} : \frac{1}{6} \mathbf{v}_{be} \times \mathbf{v}_{bd} \times \mathbf{v}_{bg}, \quad (48)$$

$$T_E^{(3)} : \frac{1}{6} \mathbf{v}_{gh} \times \mathbf{v}_{ge} \times \mathbf{v}_{gd}, \quad T_F^{(3)} : \frac{1}{6} \mathbf{v}_{fh} \times \mathbf{v}_{fd} \times \mathbf{v}_{fe}. \quad (49)$$

Here, we have assumed a positive orientation for the normal vector associated with $T_A^{(3)}$, and then insisted that all other normal vectors (for $T_B^{(3)}$ – $T_F^{(3)}$) are consistent with this orientation. Note that, we say a vector $\mathbf{n} \in \mathbb{R}^4$ has a positive orientation if $(\mathbf{p}_2 - \mathbf{p}_1) \cdot \mathbf{n} > 0$. Furthermore, we note that the generalized cross product in \mathbb{R}^4 is defined as follows

$$\mathbf{u} \times \mathbf{v} \times \mathbf{w} = \mathbf{e}_1 \begin{vmatrix} u_2 & u_3 & u_4 \\ v_2 & v_3 & v_4 \\ w_2 & w_3 & w_4 \end{vmatrix} - \mathbf{e}_2 \begin{vmatrix} u_1 & u_3 & u_4 \\ v_1 & v_3 & v_4 \\ w_1 & w_3 & w_4 \end{vmatrix} + \mathbf{e}_3 \begin{vmatrix} u_1 & u_2 & u_4 \\ v_1 & v_2 & v_4 \\ w_1 & w_2 & w_4 \end{vmatrix} - \mathbf{e}_4 \begin{vmatrix} u_1 & u_2 & u_3 \\ v_1 & v_2 & v_3 \\ w_1 & w_2 & w_3 \end{vmatrix}, \quad (50)$$

where $\mathbf{u}, \mathbf{v}, \mathbf{w} \in \mathbb{R}^4$, $\mathbf{e}_i \in \mathbb{R}^4$, and $i = 1, \dots, 4$ is the set of coordinate vectors which are 1 in the i -th coordinate direction and 0 in all other directions.

Next, we can sum over the normal vectors (Eqs. (47)–(49)) in order to construct $\mathbf{n}(\mathcal{F}^{T_\alpha})$, as follows

$$\begin{aligned} \mathbf{n}(\mathcal{F}^{T_\alpha}) &= \frac{1}{6} [\mathbf{v}_{ba} \times \mathbf{v}_{bd} \times \mathbf{v}_{be} + \mathbf{v}_{ce} \times \mathbf{v}_{ca} \times \mathbf{v}_{cd} + \mathbf{v}_{ce} \times \mathbf{v}_{cd} \times \mathbf{v}_{cf} \\ &\quad + \mathbf{v}_{be} \times \mathbf{v}_{bd} \times \mathbf{v}_{bg} + \mathbf{v}_{gh} \times \mathbf{v}_{ge} \times \mathbf{v}_{gd} + \mathbf{v}_{fh} \times \mathbf{v}_{fd} \times \mathbf{v}_{fe}] \\ &= \frac{1}{60} \left[\frac{1}{2} (-\mathbf{p}_1 \times \mathbf{p}_4 \times \mathbf{p}_5 - \mathbf{p}_2 \times \mathbf{p}_4 \times \mathbf{p}_5 + \mathbf{p}_1 \times \mathbf{p}_3 \times \mathbf{p}_5 \right. \\ &\quad \left. + \mathbf{p}_2 \times \mathbf{p}_3 \times \mathbf{p}_5 - \mathbf{p}_1 \times \mathbf{p}_3 \times \mathbf{p}_4 - \mathbf{p}_2 \times \mathbf{p}_3 \times \mathbf{p}_4) + \mathbf{p}_3 \times \mathbf{p}_4 \times \mathbf{p}_5 \right]. \quad (51) \end{aligned}$$

Thereafter, we can substitute $\mathbf{p}_1 = \mathbf{p}_2 - (\mathbf{p}_2 - \mathbf{p}_1)$ into Eq. (51), such that

$$\begin{aligned} \mathbf{n}(\mathcal{F}^{T_\alpha}) = \frac{1}{60} & \left[\mathbf{p}_3 \times \mathbf{p}_4 \times \mathbf{p}_5 + \mathbf{p}_2 \times \mathbf{p}_3 \times \mathbf{p}_5 - \mathbf{p}_2 \times \mathbf{p}_3 \times \mathbf{p}_4 - \mathbf{p}_2 \times \mathbf{p}_4 \times \mathbf{p}_5 \right. \\ & \left. + \frac{1}{2} ((\mathbf{p}_2 - \mathbf{p}_1) \times \mathbf{p}_4 \times \mathbf{p}_5 - (\mathbf{p}_2 - \mathbf{p}_1) \times \mathbf{p}_3 \times \mathbf{p}_5 + (\mathbf{p}_2 - \mathbf{p}_1) \times \mathbf{p}_3 \times \mathbf{p}_4) \right]. \end{aligned} \quad (52)$$

The quantity on the first line of Eq. (52) has special significance. In order to see this, consider the facet opposite \mathbf{p}_1 in the element T_α

$$\text{opp}_1(T_\alpha) : \text{conv}(\{\mathbf{p}_2, \mathbf{p}_3, \mathbf{p}_4, \mathbf{p}_5\}). \quad (53)$$

The spanning vectors for this facet are

$$\text{opp}_1(T_\alpha) : \mathbf{v}_{23} = \mathbf{p}_3 - \mathbf{p}_2, \quad \mathbf{v}_{24} = \mathbf{p}_4 - \mathbf{p}_2, \quad \mathbf{v}_{25} = \mathbf{p}_5 - \mathbf{p}_2. \quad (54)$$

In turn, the associated normal vector is

$$\mathbf{n}_1^{T_\alpha} = \frac{1}{6} \mathbf{v}_{23} \times \mathbf{v}_{24} \times \mathbf{v}_{25}, \quad (55)$$

or equivalently,

$$\mathbf{n}_1^{T_\alpha} = \frac{1}{6} (\mathbf{p}_3 \times \mathbf{p}_4 \times \mathbf{p}_5 + \mathbf{p}_2 \times \mathbf{p}_3 \times \mathbf{p}_5 - \mathbf{p}_2 \times \mathbf{p}_3 \times \mathbf{p}_4 - \mathbf{p}_2 \times \mathbf{p}_4 \times \mathbf{p}_5). \quad (56)$$

Here, we assume that $\mathbf{n}_1^{T_\alpha}$ has a positive orientation. Upon substituting Eq. (56) into Eq. (52), we obtain

$$\mathbf{n}(\mathcal{F}^{T_\alpha}) = \frac{1}{10} \left[\mathbf{n}_1^{T_\alpha} + \frac{1}{12} (\mathbf{p}_2 - \mathbf{p}_1) \times (\mathbf{p}_4 \times \mathbf{p}_5 - \mathbf{p}_3 \times \mathbf{p}_5 + \mathbf{p}_3 \times \mathbf{p}_4) \right]. \quad (57)$$

Setting Eq. (57) aside for the moment, we can introduce the following identities

$$\begin{aligned} & (\mathbf{p}_2 - \mathbf{p}_1) \times \mathbf{p}_3 \times \mathbf{p}_4 \\ &= (\mathbf{p}_2 - \mathbf{p}_1) \times [(\mathbf{p}_3 - \mathbf{p}_1 + \mathbf{p}_1) \times (\mathbf{p}_4 - \mathbf{p}_1 + \mathbf{p}_1)] \\ &= (\mathbf{p}_2 - \mathbf{p}_1) \times [(\mathbf{p}_3 - \mathbf{p}_1) \times (\mathbf{p}_4 - \mathbf{p}_1) + (\mathbf{p}_3 - \mathbf{p}_1) \times \mathbf{p}_1 + \mathbf{p}_1 \times (\mathbf{p}_4 - \mathbf{p}_1)], \end{aligned} \quad (58)$$

$$\begin{aligned} & (\mathbf{p}_2 - \mathbf{p}_1) \times \mathbf{p}_3 \times \mathbf{p}_5 \\ &= (\mathbf{p}_2 - \mathbf{p}_1) \times [(\mathbf{p}_3 - \mathbf{p}_1 + \mathbf{p}_1) \times (\mathbf{p}_5 - \mathbf{p}_1 + \mathbf{p}_1)] \\ &= (\mathbf{p}_2 - \mathbf{p}_1) \times [(\mathbf{p}_3 - \mathbf{p}_1) \times (\mathbf{p}_5 - \mathbf{p}_1) + (\mathbf{p}_3 - \mathbf{p}_1) \times \mathbf{p}_1 + \mathbf{p}_1 \times (\mathbf{p}_5 - \mathbf{p}_1)], \end{aligned} \quad (59)$$

$$\begin{aligned} & (\mathbf{p}_2 - \mathbf{p}_1) \times \mathbf{p}_4 \times \mathbf{p}_5 \\ &= (\mathbf{p}_2 - \mathbf{p}_1) \times [(\mathbf{p}_4 - \mathbf{p}_1 + \mathbf{p}_1) \times (\mathbf{p}_5 - \mathbf{p}_1 + \mathbf{p}_1)] \\ &= (\mathbf{p}_2 - \mathbf{p}_1) \times [(\mathbf{p}_4 - \mathbf{p}_1) \times (\mathbf{p}_5 - \mathbf{p}_1) + (\mathbf{p}_4 - \mathbf{p}_1) \times \mathbf{p}_1 + \mathbf{p}_1 \times (\mathbf{p}_5 - \mathbf{p}_1)]. \end{aligned} \quad (60)$$

Upon combining Eqs. (58)–(60), one obtains

$$\begin{aligned} & (\mathbf{p}_2 - \mathbf{p}_1) \times (\mathbf{p}_4 \times \mathbf{p}_5 - \mathbf{p}_3 \times \mathbf{p}_5 + \mathbf{p}_3 \times \mathbf{p}_4) \\ &= (\mathbf{p}_2 - \mathbf{p}_1) \times \left[(\mathbf{p}_4 - \mathbf{p}_1) \times (\mathbf{p}_5 - \mathbf{p}_1) - (\mathbf{p}_3 - \mathbf{p}_1) \times (\mathbf{p}_5 - \mathbf{p}_1) + (\mathbf{p}_3 - \mathbf{p}_1) \times (\mathbf{p}_4 - \mathbf{p}_1) \right]. \end{aligned} \quad (61)$$

We now return our attention to Eq. (57). Upon substituting Eq. (61) into Eq. (57), one obtains

$$\begin{aligned} \mathbf{n}(\mathcal{F}^{T_\alpha}) = \frac{1}{10} \left[\mathbf{n}_1^{T_\alpha} + \frac{1}{12} \left[(\mathbf{p}_2 - \mathbf{p}_1) \times (\mathbf{p}_4 - \mathbf{p}_1) \times (\mathbf{p}_5 - \mathbf{p}_1) \right. \right. \\ \left. \left. - (\mathbf{p}_2 - \mathbf{p}_1) \times (\mathbf{p}_3 - \mathbf{p}_1) \times (\mathbf{p}_5 - \mathbf{p}_1) \right. \right. \\ \left. \left. + (\mathbf{p}_2 - \mathbf{p}_1) \times (\mathbf{p}_3 - \mathbf{p}_1) \times (\mathbf{p}_4 - \mathbf{p}_1) \right] \right]. \end{aligned} \quad (62)$$

The rightmost terms inside the parentheses of Eq. (62) are associated with the opposite facets of T_α . In particular, we can introduce three such opposite facets

$$\text{opp}_3(T_\alpha) : \text{conv}(\{\mathbf{p}_1, \mathbf{p}_2, \mathbf{p}_4, \mathbf{p}_5\}), \quad (63)$$

$$\text{opp}_4(T_\alpha) : \text{conv}(\{\mathbf{p}_1, \mathbf{p}_2, \mathbf{p}_3, \mathbf{p}_5\}), \quad (64)$$

$$\text{opp}_5(T_\alpha) : \text{conv}(\{\mathbf{p}_1, \mathbf{p}_2, \mathbf{p}_3, \mathbf{p}_4\}). \quad (65)$$

The associated normal vectors are given by

$$\mathbf{n}_3^{T_\alpha} = \frac{1}{6} (\mathbf{p}_2 - \mathbf{p}_1) \times (\mathbf{p}_4 - \mathbf{p}_1) \times (\mathbf{p}_5 - \mathbf{p}_1), \quad (66)$$

$$\mathbf{n}_4^{T_\alpha} = \frac{1}{6} (\mathbf{p}_2 - \mathbf{p}_1) \times (\mathbf{p}_5 - \mathbf{p}_1) \times (\mathbf{p}_3 - \mathbf{p}_1), \quad (67)$$

$$\mathbf{n}_5^{T_\alpha} = \frac{1}{6} (\mathbf{p}_2 - \mathbf{p}_1) \times (\mathbf{p}_3 - \mathbf{p}_1) \times (\mathbf{p}_4 - \mathbf{p}_1), \quad (68)$$

where the orientations of these vectors are taken to be consistent with $\mathbf{n}_1^{T_\alpha}$. Next, upon substituting Eqs. (66)–(68) into Eq. (62), we obtain

$$\mathbf{n}(\mathcal{F}^{T_\alpha}) = \frac{1}{10} \left[\mathbf{n}_1^{T_\alpha} + \frac{1}{2} \left(\mathbf{n}_3^{T_\alpha} + \mathbf{n}_4^{T_\alpha} + \mathbf{n}_5^{T_\alpha} \right) \right]. \quad (69)$$

Thereafter, we can show that the contributions from $\mathbf{n}_3^{T_\alpha}$, $\mathbf{n}_4^{T_\alpha}$, and $\mathbf{n}_5^{T_\alpha}$ in Eq. (69) are canceled by neighboring pentatopes T_β , T_γ , and T_δ . In particular, we find that

$$\mathbf{n}(\mathcal{F}^{T_\beta}) = \frac{1}{10} \left[\mathbf{n}_1^{T_\beta} + \frac{1}{2} \left(\mathbf{n}_3^{T_\beta} + \mathbf{n}_4^{T_\beta} + \mathbf{n}_6^{T_\beta} \right) \right], \quad (70)$$

$$\mathbf{n}(\mathcal{F}^{T_\gamma}) = \frac{1}{10} \left[\mathbf{n}_1^{T_\gamma} + \frac{1}{2} \left(\mathbf{n}_3^{T_\gamma} + \mathbf{n}_5^{T_\gamma} + \mathbf{n}_7^{T_\gamma} \right) \right], \quad (71)$$

$$\mathbf{n}(\mathcal{F}^{T_\delta}) = \frac{1}{10} \left[\mathbf{n}_1^{T_\delta} + \frac{1}{2} \left(\mathbf{n}_4^{T_\delta} + \mathbf{n}_5^{T_\delta} + \mathbf{n}_8^{T_\delta} \right) \right], \quad (72)$$

and furthermore

$$\mathbf{n}_3^{T_\alpha} = -\mathbf{n}_8^{T_\delta}, \quad \mathbf{n}_4^{T_\alpha} = -\mathbf{n}_7^{T_\gamma}, \quad \mathbf{n}_5^{T_\alpha} = -\mathbf{n}_6^{T_\beta}. \quad (73)$$

Therefore, the only net contribution from T_α to the summation

$$\mathbf{n}(\mathcal{F}^{T_\alpha}) + \mathbf{n}(\mathcal{F}^{T_\beta}) + \mathbf{n}(\mathcal{F}^{T_\gamma}) + \mathbf{n}(\mathcal{F}^{T_\delta}), \quad (74)$$

is

$$\frac{1}{10} \mathbf{n}_1^{T_\alpha}. \quad (75)$$

Since $T_\alpha = \text{conv}(\{\mathbf{p}_1, \mathbf{p}_2, \mathbf{p}_3, \mathbf{p}_4, \mathbf{p}_5\})$ is a generic 4-simplex which shares the edge $\mathbf{p}_2 - \mathbf{p}_1$, we conclude that T_β , T_γ , and T_δ make similar net contributions

$$\frac{1}{10} \mathbf{n}_1^{T_\beta}, \frac{1}{10} \mathbf{n}_1^{T_\gamma}, \frac{1}{10} \mathbf{n}_1^{T_\delta}. \quad (76)$$

Summing over the contributions from each pentatope that shares the edge $\mathbf{p}_2 - \mathbf{p}_1$ produces the desired result (Eq. (22)). ◀

► **Remark 7 (Boundary Considerations).** Theorem 6 needs to be modified slightly if \mathbf{p}_j is a boundary point. In this case, Eq. (22) can be changed as follows

$$\mathbf{n}_{jk} = \frac{1}{10} \left(\sum_{T \in \{\mathbb{T}_{jk}^{(4)}\}} \mathbf{n}_j^T + \frac{1}{2} \sum_{B \in \{\mathbb{T}_{jk}^{(3)} \cap \partial\Omega\}} \mathbf{n}_B \right), \quad (77)$$

where \mathbf{n}_B is the outward-pointing normal vector of the boundary 3-simplex B .

► **Remark 8 (Implementation Details).** We recommend implementing Eq. (22) from Theorem 6 and Eq. (77) from Remark 7 as follows:

- Loop over each 4-simplex in the triangulation.
- For each 4-simplex T , loop over the 3-facets.
- For each facet, identify the vertices of the facet in the global numbering system, e.g. $\mathbf{p}_{i_1}, \mathbf{p}_{i_2}, \mathbf{p}_{i_3}$, and \mathbf{p}_{i_4} , along with the vertex opposite the facet, e.g. \mathbf{p}_{i_5} .
- Update the directed-hyperarea vector for the edge $\mathbf{p}_k - \mathbf{p}_j$ using each vertex of the facet

$$\mathbf{n}_{jk} = \mathbf{n}_{jk} + \frac{1}{10} \mathbf{n}_j^T, \quad (78)$$

where $(j, k) \in \{(r, s) \in \{i_1, i_2, i_3, i_4, i_5\}^2 \mid r < s\}$. Note that we store only one directed-hyperarea vector per edge, \mathbf{n}_{jk} in the direction from the smaller node number to the larger node number (i.e. $j < k$), because its counterpart \mathbf{n}_{kj} is given by $\mathbf{n}_{kj} = -\mathbf{n}_{jk}$.

- Loop over each boundary 3-simplex B .
- For each boundary facet, identify the vertices of the facet in the global numbering system, e.g. $\mathbf{p}_{i_1}, \mathbf{p}_{i_2}, \mathbf{p}_{i_3}$ and \mathbf{p}_{i_4} .
- Correct the directed-hyperarea vector for the edge $\mathbf{p}_k - \mathbf{p}_j$ using each vertex of the boundary facet

$$\mathbf{n}_{jk} = \mathbf{n}_{jk} + \frac{1}{20} \mathbf{n}_B, \quad (79)$$

where $(j, k) \in \{(r, s) \in \{i_1, i_2, i_3, i_4\}^2 \mid r < s\}$.

► **Remark 9 (Verification Details).** Once the directed-hyperarea vectors have been computed using the procedure of Remark 8, they can be verified as follows:

- Create node vectors \mathbf{a}_j associated with each node \mathbf{p}_j .
- Loop over each edge $\mathbf{p}_k - \mathbf{p}_j$ ($j < k$) of the triangulation.
- Update the node vectors

$$\mathbf{a}_j = \mathbf{a}_j + \mathbf{n}_{jk}, \quad \mathbf{a}_k = \mathbf{a}_k - \mathbf{n}_{jk} = \mathbf{a}_k + \mathbf{n}_{kj}. \quad (80)$$

- Loop over each boundary 3-simplex B .
- For each boundary facet, identify the vertices of the facet in the global numbering system, e.g. $\mathbf{p}_{i_1}, \mathbf{p}_{i_2}, \mathbf{p}_{i_3}$ and \mathbf{p}_{i_4} .
- Update the node vector

$$\mathbf{a}_j = \mathbf{a}_j + \frac{1}{5} \mathbf{n}_B, \quad (81)$$

where $j = i_1, i_2, i_3$ and i_4 .

When we complete the procedure above, if each $\mathbf{a}_j = \mathbf{0}$, then we have established the correctness of the implementation.

5 Conclusion

In this paper, we provide important geometric formulas for node-centered, edge-based space-time methods on triangulations in \mathbb{R}^4 . These formulas allow us to compute two key ingredients of the median-dual tessellation: i) a relationship between the hypervolume of each median-dual region and the directed-hyperarea vectors, (see Theorem 5); and ii) a relationship between the directed-hyperarea vectors and the facet normals of the associated simplices, (see Theorem 6). These ingredients enable us to create a node-centered, edge-based scheme which (in the interior of the domain) only stores and operates on edge data, in the form of directed-hyperarea vectors. More precisely, we can compute the directed-hyperarea vectors for each edge as a pre-processing step, and then calculate the hypervolume of each median-dual region on-the-fly. As a result, computing the residual at each interior node is simply a matter of evaluating the appropriate solution and numerical flux functions (and accumulating any source-term contributions), and accessing the corresponding pre-computed directed-hyperarea vectors for each edge. Furthermore, Remark 9 suggests an explicit method for looping over boundary elements, and enforcing the necessary boundary conditions. However, accuracy-preserving boundary flux quadrature formulas still need to be derived for a node-centered edge-based scheme to achieve second-order and third-order accuracy at boundary nodes in 4D. In addition, there is still interest in extending the proof of Theorem 6 to $d > 4$, and proving Conjecture 4. Such endeavors would be of practical use for higher-dimensional problems, for example, those in the field of radiation transport.

References

- 1 R. Abgrall and S. Karni. Computations of compressible multifluids. *Journal of Computational Physics*, 169(2):594–623, 2001.
- 2 W. K Anderson, R. T. Biedron, J.-R. Carlson, J. M. Derlaga, B. Diskin, C. T. Druypr Jr., P. A. Gnoffo, D. P. Hammond, K. E. Jacobson, W. T. Jones, B. Kleb, E. M. Lee-Rausch, Y. Liu, G. C. Nastac, E. J. Nielsen, E. M. Padway, M. A. Park, C. L. Rumsey, J. L. Thomas, K. B. Thompson, A. Walden, L. Wang, S. L. Wood, W. A. Wood, and X. Zhang. FUN3D manual: 14.1. *NASA-NASA/TM--20240006306*, June 2024.
- 3 F. Aurenhammer. Power diagrams: properties, algorithms and applications. *SIAM Journal on Computing*, 16(1):78–96, 1987.
- 4 T. J. Barth. Numerical aspects of computing viscous high Reynolds number flows on unstructured meshes. AIAA Paper 91-0721, 1991.
- 5 T. J. Barth. Aspects of unstructured grids and finite-volume solvers for the Euler and Navier-Stokes equations, 1992.
- 6 G. Belda-Ferrín, E. Ruiz-Gironés, A. Gargallo-Peiró, and X. Roca. Conformal marked bisection for local refinement of n-dimensional unstructured simplicial meshes. *Computer-Aided Design*, 154:103419, 2023.

- 7 W. Blaschke. Vorlesungen über differentialgeometrie III, die grundlehren der mathematischen wissenschaften, 1929.
- 8 J.-D. Boissonnat, F. Chazal, and M. Yvinec. *Geometric and topological inference*, volume 57. Cambridge University Press, 2018.
- 9 A. Bowyer. Computing Dirichlet tessellations. *The Computer Journal*, 24(2):162–166, 1981.
- 10 P. C. Caplan, R. Haimes, D. L. Darmofal, and M. C. Galbraith. Four-dimensional anisotropic mesh adaptation. *Computer-Aided Design*, 129:102915, 2020.
- 11 P. C. D. Caplan. *Four-dimensional anisotropic mesh adaptation for spacetime numerical simulations*. PhD thesis, Massachusetts Institute of Technology, 2019.
- 12 C. T. Chan and K. Anastasiou. An automatic tetrahedral mesh generation scheme by the advancing front method. *Communications in Numerical Methods in Engineering*, 13(1):33–46, 1997.
- 13 H. S. M. Coxeter. Discrete groups generated by reflections. *Annals of Mathematics*, 35(3):588–621, 1934.
- 14 H. S. M. Coxeter. Geometry revisited. *The Mathematical Association of America*, 1967.
- 15 B. Diskin and J. L. Thomas. Effects of mesh regularity on accuracy of finite-volume schemes. In *50th AIAA Aerospace Sciences Meeting*, AIAA Paper 2012-0609, Nashville, Tennessee, 2012.
- 16 P. Eliasson. EDGE, a Navier-Stokes solver, for unstructured grids. Technical Report FOI-R-0298-SE, Swedish Defence Research Agency, December 2001.
- 17 L. Fezoui and B. Stouffle. A class of implicit upwind schemes for Euler simulations with unstructured meshes. *Journal of Computational Physics*, 84:174–206, 1989.
- 18 S. Fortune. A sweepline algorithm for Voronoi diagrams. In *Proceedings of the Second Annual Symposium on Computational Geometry*, pages 313–322, 1986.
- 19 H. Freudenthal. Simplicialzerlegungen von beschränkter flachheit. *Annals of Mathematics*, 43(3):580–582, 1942.
- 20 P. J. Frey, H. Borouchaki, and P.-L. George. 3D Delaunay mesh generation coupled with an advancing-front approach. *Computer Methods in Applied Mechanics and Engineering*, 157(1-2):115–131, 1998.
- 21 E. Gaburro, W. Boscheri, S. Chiochetti, and M. Ricchiuto. Discontinuous Galerkin schemes for hyperbolic systems in non-conservative variables: quasi-conservative formulation with subcell finite volume corrections. *Computer Methods in Applied Mechanics and Engineering*, 431:117311, 2024.
- 22 S. Gao, W. G. Habashi, M. Fossati, D. Isola, and G. S. Baruzzi. Finite-element formulation of a Jacobian-free solver for supersonic viscous flows on hybrid grids. In *55th AIAA Aerospace Sciences Meeting*, AIAA Paper 2017-0085, Grapevine, Texas, 2017.
- 23 P. L. George and E. Seveno. The advancing-front mesh generation method revisited. *International Journal for Numerical Methods in Engineering*, 37(21):3605–3619, 1994.
- 24 A. Haselbacher and J. Blazek. Accurate and efficient discretization of Navier-Stokes equations on mixed grids. *AIAA Journal*, 38(11):2094–2102, 2000. URL: <http://arc.aiaa.org/doi/abs/10.2514/2.871>.
- 25 E. Johnsen and F. Ham. Preventing numerical errors generated by interface-capturing schemes in compressible multi-material flows. *Journal of Computational Physics*, 231(17):5705–5717, 2012.
- 26 A. Katz and V. Sankaran. Mesh quality effects on the accuracy of CFD solutions on unstructured meshes. *Journal of Computational Physics*, 230:7670–7686, 2011. doi: 10.1016/j.jcp.2011.06.023.
- 27 A. Katz and V. Sankaran. An efficient correction method to obtain a formally third-order accurate flow solver for node-centered unstructured grids. *Journal of Scientific Computing*, 51:375–393, 2012. doi:10.1007/s10915-011-9515-1.
- 28 P. P. Klein. The insphere of a tetrahedron. *Applied Mathematics*, 11:601–612, 2020.

- 29 T. Kozubskaya, I. Abalakin, A. Dervieux, and H. Ouvrard. Accuracy improvement for finite-volume vertex-centered schemes solving aeroacoustics problems on unstructured meshes. In *16th AIAA/CEAS Aeroacoustics Conference*, AIAA Paper 2010-3933, 2010.
- 30 N. Kroll, M. Abu-Zurayk, D. Dimitrov, T. Franz, T. Führer, T. Gerhold, S. Görtz, R. Heinrich, C. Ilic, J. Jepsen, J. Jägersküpper, M. Kruse, A. Krumbein, S. Langer, D. Liu, R. Liepelt, L. Reimer, M. Ritter, A. Schwöppe, J. Scherer, F. Spiering, R. Thormann, V. Togiti, D. Vollmer, and J.-H. Wendisch. DLR Project Digital-X: Towards virtual aircraft design and flight testing based on high-fidelity methods. *CEAS Aeronautical Journal*, 7(1):3–27, March 2016. doi:10.1007/s13272-015-0179-7.
- 31 Y. Liu and H. Nishikawa. Third-order inviscid and second-order hyperbolic Navier-Stokes solvers for three-dimensional inviscid and viscous flows. In *46th AIAA Fluid Dynamics Conference*, AIAA Paper 2016-3969, Washington, D.C., 2016.
- 32 S. H. Lo. Dynamic grid for mesh generation by the advancing front method. *Computers & Structures*, 123:15–27, 2013.
- 33 R. Löhner and P. Parikh. Generation of three-dimensional unstructured grids by the advancing-front method. *International Journal for Numerical Methods in Fluids*, 8(10):1135–1149, 1988.
- 34 H. Luo, J. D. Baum, and R. Löhner. High-reynolds number viscous flow computations using an unstructured-grid method. In *42nd AIAA Aerospace Sciences Meeting*, AIAA Paper 2004-1103, Reno, NV, 2004.
- 35 Y. Lv and M. Ihme. Discontinuous Galerkin method for multicomponent chemically reacting flows and combustion. *Journal of Computational Physics*, 270:105–137, 2014.
- 36 D. J. Mavriplis. An advancing front Delaunay triangulation algorithm designed for robustness. *Journal of Computational Physics*, 117(1):90–101, 1995.
- 37 D. J. Mavriplis and M. Long. NSU3D results for the fourth AIAA drag prediction workshop. AIAA Paper 2010-4363, 2010.
- 38 P. Möller and P. Hansbo. On advancing front mesh generation in three dimensions. *International Journal for Numerical Methods in Engineering*, 38(21):3551–3569, 1995.
- 39 Y. Nakashima, N. Watanabe, and H. Nishikawa. Development of an effective implicit solver for general-purpose unstructured CFD software. In *The 28th Computational Fluid Dynamics Symposium*, C08-1, Tokyo, Japan, 2014.
- 40 M. Neumüller and O. Steinbach. Refinement of flexible space–time finite element meshes and discontinuous Galerkin methods. *Computing and Visualization in Science*, 14(5):189–205, 2011.
- 41 H. Nishikawa. Beyond interface gradient: A general principle for constructing diffusion schemes. In *40th AIAA Fluid Dynamics Conference and Exhibit*, AIAA Paper 2010-5093, Chicago, IL, 2010.
- 42 H. Nishikawa. Accuracy-preserving boundary flux quadrature for finite-volume discretization on unstructured grids. *Journal of Computational Physics*, 281:518–555, 2015.
- 43 H. Nishikawa. A face-area-weighted centroid formula for reducing grid skewness and improving convergence of edge-based solver on highly-skewed simplex grids. In *AIAA Scitech 2020 Forum*, AIAA Paper 2020-1786, Orlando, FL, 2020.
- 44 H. Nishikawa. An efficient implementation of edge-based discretization without forming dual control volumes. *International Journal for Numerical Methods in Fluids*, 2024. under review.
- 45 H. Nishikawa and Y. Liu. Accuracy-preserving source term quadrature for third-order edge-based discretization. *Journal of Computational Physics*, 344:595–622, 2017.
- 46 H. Nishikawa and Y. Liu. Hyperbolic Navier-Stokes method for high-Reynolds-number boundary-layer flows. In *55th AIAA Aerospace Sciences Meeting*, AIAA Paper 2017-0081, Grapevine, Texas, 2017.
- 47 E. Pärt-Enander and B. Sjögren. Conservative and non-conservative interpolation between overlapping grids for finite volume solutions of hyperbolic problems. *Computers & fluids*, 23(3):551–574, 1994.

- 48 A. Peyvan, D. Li, J. Komperda, and F. Mashayek. Oscillation-free nodal discontinuous spectral element method for the simulation of compressible multicomponent flows. *Journal of Computational Physics*, 452:110921, 2022.
- 49 T. Smith, C. Ober, and A. Lorber. SIERRA/Premo-A new general purpose compressible flow simulation code. In *32nd AIAA Fluid Dynamics Conference and Exhibit*, AIAA Paper 2002-3292, St. Louis, MO, 2002.
- 50 G. Voronoi. Nouvelles applications des paramètres continus à la théorie des formes quadratiques. deuxième mémoire. recherches sur les paralléloèdres primitifs. *Journal für die reine und angewandte Mathematik (Crelles Journal)*, 1908(134):198–287, 1908.
- 51 G. Voronoi. Nouvelles applications des paramètres continus à la théorie des formes quadratiques. premier mémoire. sur quelques propriétés des formes quadratiques positives parfaites. *Journal für die reine und angewandte Mathematik (Crelles Journal)*, 1908(133):97–102, 1908.
- 52 D. F. Watson. Computing the n-dimensional Delaunay tessellation with application to Voronoi polytopes. *The Computer Journal*, 24(2):167–172, 1981.